The modulation and reconstruction of a BiO layer of cuprate Bi2212



2011 Supercond. Sci. Technol. 24 105007

(http://iopscience.iop.org/0953-2048/24/10/105007)

Supercond. Sci. Technol. **24** (2011) 105007 (7pp) doi:10.1088/0953-2048/24/10/105007

# The modulation and reconstruction of a BiO layer of cuprate Bi2212

**Wei Fan and Z Zeng**

Key Laboratory of Materials Physics, Institute of Solid State Physics, Hefei Institutes of Physical Sciences, Chinese Academy of Sciences, 230031-Hefei, People's Republic of China

Received 23 May 2011, in final form 3 July 2011
Published 23 August 2011
Online at stacks.iop.org/SUST/24/105007

**Abstract**

Studies based on *ab initio* density functional theory show that the modulated structures of BiO surfaces of cuprate Bi2212 superconductors are spontaneously formed and closely related to the reconstructions of BiO surfaces. The reconstructions of BiO layers occur both on the surface and in the bulk, accompanied with the formations of BiO-zigzag chains and $Bi_2O_2$ quadrilaterals. The structural modulations of the BiO surface are along the *b* axis, perpendicular to the BiO-zigzag chains along the *a* axis. Our calculations provide a unified understanding of the formation of modulating structures in Bi2212. Another interesting result is that electronic structures of BiO surfaces are significantly influenced by the $CuO_2$ layer beneath because of the structural modulations and reconstructions.

(Some figures in this article are in colour only in the electronic version)

## 1. Introduction

The copper oxide high-temperature superconductor $Bi_2Sr_2CaCu_2O_{8+\delta}$ (Bi2212) has been studied extensively since its discovery [1] because its temperature of transition ($T_c$) to a superfluid is higher than the boiling point of liquid nitrogen (77 K). A significant structure characteristic of Bi2212 is the weak coupling between BiO layers. This makes it easy to produce clean BiO surfaces, so some surface techniques, such as photoemission and scanning tunneling microscopy ones, can be used to study superconducting properties. The observations using x-ray, neutron, and electron diffraction and scanning tunneling microscopy have found incommensurate modulations with length period $4.7b_0$–$4.8b_0$ ($b_0$ is the lattice constant along the *b* direction) [2–5], which generally change on introducing external impurities [6]. Early explanations of the incommensurate modulations were based on the analysis of x-ray diffractions and told us that the modulations along so-called one-dimensional BiO chains are created by the bridging zones along BiO chains or the extra oxygen atoms between nearest BiO chains [7–12]. However some of observations claimed that the structural modulations were spontaneously formed, driven by the bond-length misfit between the BiO layer and the neighboring perovskite-like structure [13, 14]. The observations of scanning tunneling microscopy have provided new information on the modulations of BiO surfaces. One-dimensional S-like structures [15] or 'missing-row' structures [16] are found, but modulations over about five lattice periods are perpendicular to the direction of 'missing-row' or S-like structures. The S-like structures seem to be atom-dilute regions. It is unclear whether they are formed via a number of atoms being missing or via the splitting of BiO surfaces induced by large strains between the BiO surface and underlying atomic layers. The modulations of the BiO surface (found from STM experiments) and the modulations in the bulk have almost the same modulating period, $4.7b_0$–$4.8b_0$, implying the same formation mechanism. To reconcile the explanations of different experimental techniques, deeper understanding of the incommensurate modulations is required [17].

The *ab initio* density functional theory had been widely used to calculate the electronic structures and atomic structures of Bi2212 and other cuprate superconductors. The Fermi surfaces of optimally doped Bi2212 obtained in the calculations of the band structure of Bi2212 are in good consistency with ARPES spectrum [18] although some BiO pockets were not found experimentally in ARPES spectra. Theoretically, the effects of structural optimization [18] and interstitial oxygen doping [19] can remove or weaken these BiO pockets. Only a few calculations of *ab initio* density functional theory had reported results on the forming mechanism of modulation structures of Bi2212 [20, 21]. In one of these works [21], the structural modulations of the BiO layer had been found by using a large simulation cell. At the current stage more theoretical calculations are needed to clarify

 

the nature of the incommensurate modulation of Bi2212 and its relation to high-temperature superconductivity.

In this work, we study the mechanism forming the incommensurate modulations of Bi2212 on the basis of calculations using *ab initio* density functional theory. We find that the structural modulations along the $b$ axis on the BiO surface are formed spontaneously, and are closely related to the reconstructions of BiO layers found both on the surface and in the bulk. The features of the electronic structure of the $CuO_2$ layer beneath appear on the BiO surface due to the structural modulations and reconstructions. The narrow conducting strip on the BiO surface in our calculations is very interesting because it connects to the electronic structure of the $CuO_2$ layer beneath.

## 2. Methods of the theory and simulation

The plane-wave basis is used to solve the Kohn–Sham equation in this work [22]. The interactions between ion cores and valence electrons are treated in the framework of the projector-augmented-wave method [23, 22]. The exchange–correlation functional adopted in this work is based on the generalized gradient approximation (GGA) [24]. The initial structure is the averaged structure in orthorhombic symmetry with lattice constants $a_0 \sim b_0 = 5.4$ Å and $c_0 = 30.9$ Å. The five atomic layers (two SrO layers, two $CuO_2$ layers and one Ca layer) sandwiching between two BiO layers form the so-called slab structure as the basic structure unit of Bi2212 crystal. Two such slab units stacking along $c$ axis, with one translating by $(a_0/2)\hat{x} + (b_0/2)\hat{y} + (c_0/2)\hat{z}$ related to the other, compose a complete unit cell of Bi2212 crystal. The initial structures with large simulation cells in the following section will be fully relaxed as regards the coordinates of atoms, volumes and shapes of supercells to reach the locally stable configurations. The local corrections of Coulomb-correlation effects of d electrons of Cu atoms are ignored in this work. The standard LDA approximation of density functional theory can produce the main figure for the Fermi surface of Bi2212 at the optimal doping level [18]. The energy cutoff of the plane waves is about 400 eV. The spin polarizations are included; however the atoms in our simulation cell have no magnetic moments after we have performed self-consistent calculations.

## 3. Modulations and reconstructions of BiO surfaces

As the first step, we optimize the basic slab structure with a total of 300 atoms by using the conjugate-gradient method. The sizes of the slab along $a$ and $b$ axes are $2a_0$ and $5b_0$ respectively. There is empty space about 12 Å in size between two BiO surfaces under periodic boundary conditions along the $c$ axis. When we optimize the structure of the slab, the $\Gamma$ point is used to sample the Brillouin zone in corresponding calculations of the electronic structure. The optimized structure is illustrated in figure 1(a). We can find from this figure that all atomic layers are bent, with sinusoidal shapes. The amplitude of the sinusoidal wave of the Bi atoms along $c$ is about 0.2 Å which is smaller than the 0.4 Å in the

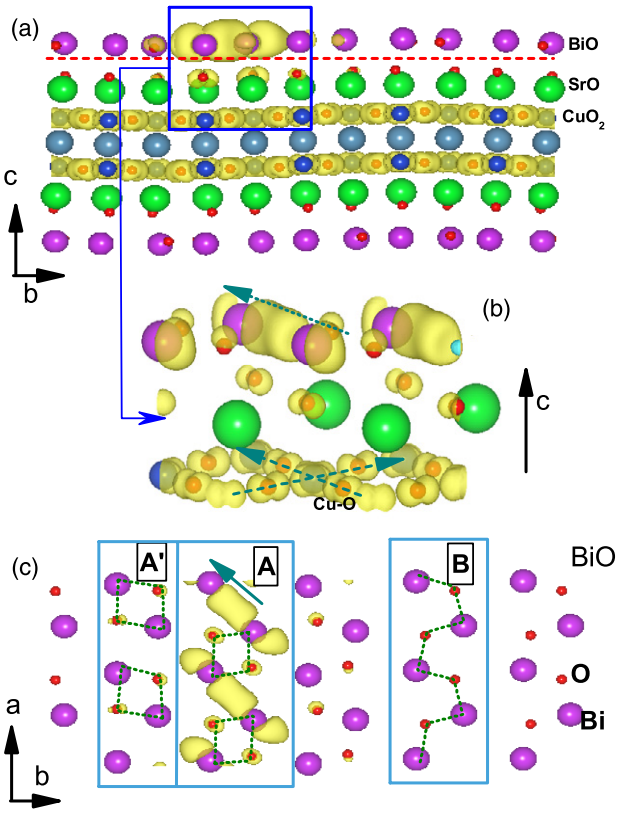


**Figure 1.** (a) The long-range modulation of the BiO surface. The Bi2212 slab is projected along the $a$ axis (side view). The local density of states (LDOS) near the Fermi energy (±50 meV) are plotted using the iso-surface with the iso-value 0.001 (1 $Å^{-3}$). The dotted line is a guide to show the modulation of the BiO surface. (b) A locally enlarged view of the squared area in (a). The dashed arrows point in the directions of Cu–O bonds in the $CuO_2$ layer. (c) The same as (a) but showing the structure and LDOS for the top BiO layer projected along the $c$ axis (top view). The small balls are oxygen atoms.

experimental model that was refined using the patterns of x-ray diffraction [2]. The sinusoidal modulated structure had been found in a previous report using the same methods [21]. In this work, the size along the $a$ axis is larger than that in [21], so we have new results to present. In figure 1(c) we plot the optimized structure of the BiO surface. The BiO-zigzag chains of type **B** along the $a$ direction are found in our calculations, and are similar to the bridging zone of BiO chains refined from the patterns of x-ray diffraction [7, 12]. The $Bi_2O_2$ quadrilaterals in our calculations are aligned along the $a$ direction. These $Bi_2O_2$ quadrilaterals form a region of deformed rock-salt structure with dense distributions of Bi atoms and O atoms. The basic units of the BiO-zigzag chain and $Bi_2O_2$ quadrilateral are the basic units of the BiO chain refined from the patterns of x-ray diffractions [7, 12]. It is obvious that the modulation is perpendicular to the BiO-zigzag chains. This is contrary to the early model, which claimed that the modulations are along BiO chains and are formed by inserting extra oxygen atoms in the space between these BiO chains [9] or by creating bridging zones along BiO chains [7].

In figures 1(a)–(c), we plot the spatially distributed LDOS (local density of states) with energies ±50 meV around the

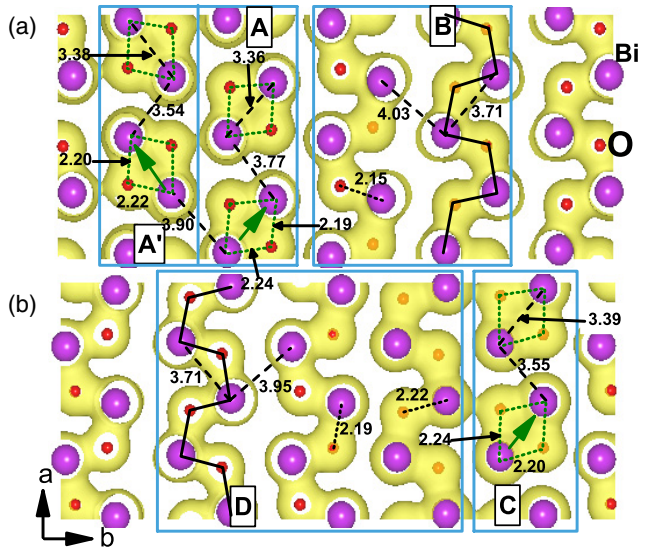


**Figure 2.** The structure and electronic density on the top (a) and bottom (b) BiO layers. We clearly reproduce the reconstruction of BiO surfaces by the formation of BiO-zigzag chains and $Bi_2O_2$ quadrilaterals. The iso-surfaces are plotted using the full densities of valence electrons with iso-value 0.02 (1 $Å^{-3}$).

Fermi energy. We can see that BiO-zigzag chain B is in an insulating state and the $Bi_2O_2$ quadrilaterals in column A are in a conducting state in the top BiO layer. The bottom BiO layer is in an insulating state. A narrow conducting strip forms in the almost insulating BiO surface. As we expect, the main conducting electrons are contributed by the $CuO_2$ planes. The apical oxygen atoms in the SrO layer near the $Bi_2O_2$ quadrilaterals make few contributions to the conducting electrons. These apical oxygen atoms move along the $c$ axis and closer to the BiO layer. Figure 1(b) shows an enlarged view of the squared area in figure 1(a) but viewing along a different direction. We can see that electron clouds of the BiO surface elongate parallel to the Cu–O bond in the $CuO_2$ layer although there is a SrO layer between them. The distribution of electronic densities around the Fermi energy in the BiO surface is very sensitively dependent on the local structure of the BiO surface because the column A′ has similar structure to column A; however there are no distributions of conducting electrons in column A′.

In figure 2 we present the structures of the top and bottom BiO surfaces and the full density of valence electrons, so we can see how Bi atoms and O atoms form chemical bonds. The BiO-zigzag chains and $Bi_2O_2$ quadrilaterals are also found in the bottom BiO surface. The difference is that the top BiO surface has two nearest-neighbor touching $Bi_2O_2$ columns labeled A and A′, and there is only one $Bi_2O_2$ column, labeled C, in the bottom surface. The region A + A′ with dense distributions of Bi atoms and O atoms in the top surface has twice the width as compared with the dense region C in the bottom surface. Thus our results mean that the width of the dense region of Bi atoms and O atoms is essential for forming an electronic conducting channel. The insulating regions near BiO-zigzag chains labeled B and D have lower densities of Bi atoms and O atoms than regions A + A′ and C. Some typical distances in BiO surfaces are presented in figure 2. The shortest Bi–Bi distance of initial non-relaxed structures is about 3.8 Å. For the optimized structure, the Bi–Bi distances of the intra-BiO-zigzag (inter-BiO-zigzag) chains and $Bi_2O_2$ quadrilaterals are shorter (longer) than 3.8 Å. Thus the dense regions and diluted regions for Bi atoms and O atoms form the structural modulations of BiO surfaces.

In order to illustrate the influence of structural optimization on the electronic structure of the BiO surface, we plot the densities of states of the top and bottom surfaces in figure 3.

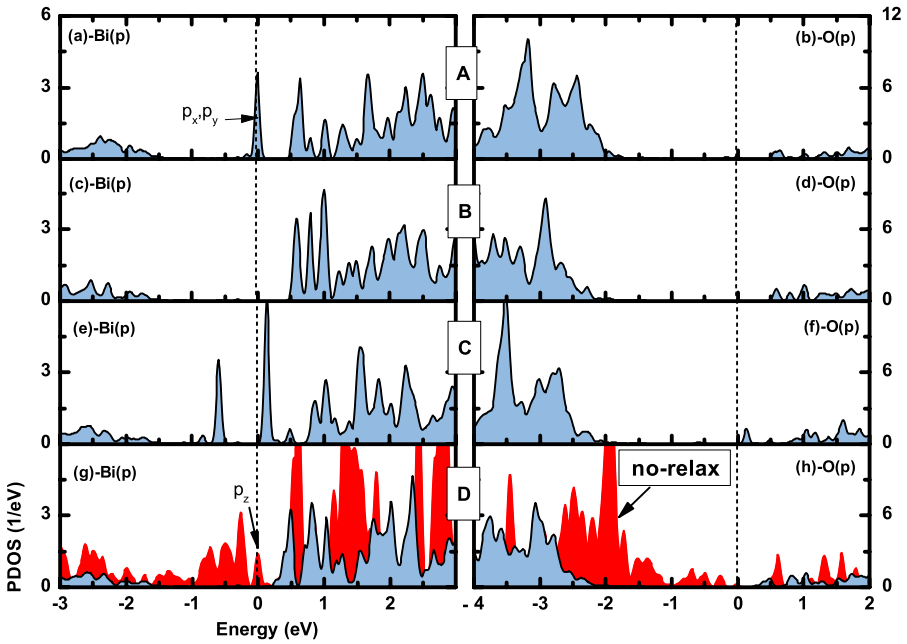


**Figure 3.** The partial density of states (PDOS) of BiO-zigzag chains and $Bi_2O_2$ quadrilaterals shown in figure 2 within the regions labeled A, B, C and D respectively. The PDOS of typical Bi atoms and O atoms in the non-relaxed structure are plotted in (g) and (h) respectively for comparison.

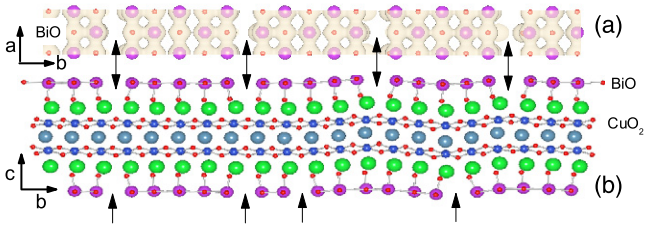


**Figure 4.** The relaxed structure of Bi2212 slabs with the sizes $10b_0$ along the $b$ direction and $a_0$ along the $a$ direction: (a) the top view and (b) the side view. The vertical arrows indicate the surface-splitting positions or the 'missing-row' positions.

Compared with the non-relaxed structure case, the density of states at the Fermi energy increases in column A, but for other regions of the BiO surface, it sharply decreases. For the density of states of Bi atoms in column A, the peaks at the Fermi energy are characterized by $p_z$ for the non-relaxed structures in figure 3(g) and by $p_x$ and $p_y$ for the relaxed structures in figure 3(a), which are consistent with the results of LAPW + lo method (full-potential linearized augmented plane-wave plus local orbitals method) [18]. For the non-relaxed structure the p electrons of Bi atom form anti-bonding orbitals with the nearest O atoms (pp$\pi^*$ bonds with O atoms on the BiO surface and pp$\sigma^*$ bonds with the apex O atoms in the SrO layer). For the relaxed structure, the peak at the Fermi energy represents the p electrons of the Bi atom forming pp$\sigma$ bonds with the p electrons of the next-nearest-neighbor Bi atoms of different quadrilaterals in the BiO layer. From figure 1(b) we can see that the pp$\sigma$ bond between Bi atoms in column A is parallel to the Cu–O bond in the $CuO_2$ layers. The $p_x$ and $p_y$ characters of the peak are closely related to the p orbitals of O atoms in the $CuO_2$ layer.

Column C in the bottom BiO layer has a similar structure to column A; there are two high peaks in the gap shown in figure 3(e), one peak above and very close to the Fermi energy and the other below the Fermi energy. It is plausible that the Fermi energy may pin at one of the two peaks through local structural modification. The columns B and D are insulating and there are no significant peaks in the gaps in figures 3(c) and (g), which is consistent with the results for the spatial LDOS in figure 1(a). Thus our results have indicated that the reconstructions of the BiO surface induce the almost insulating BiO surface with a narrow conducting strip that is influenced by the electronic structures and geometric structures of the $CuO_2$ layer beneath, shown in figures 1(b) and (c). In our results, the one-dimensional conducting strips are on the BiO layers and the $CuO_2$ layers are made up of almost homogeneously conducting electrons; this is very different from the findings from the analysis of experiments: that there are one-dimensional conducting strips on $CuO_2$ layers [25].

The experimental modulation period along the $b$ direction is about $4.7b_0$–$4.8b_0$, close to $5b_0$. Thus to reliably study the spontaneously modulated phenomenon, at least $10b_0$ length along the $b$ axis is needed. A slab of 300 atoms with size $1a_0 \times 10b_0$ on the $a$–$b$ plane is used. Other features of the slab are the same as those of the $2a_0 \times 5b_0$ slab.

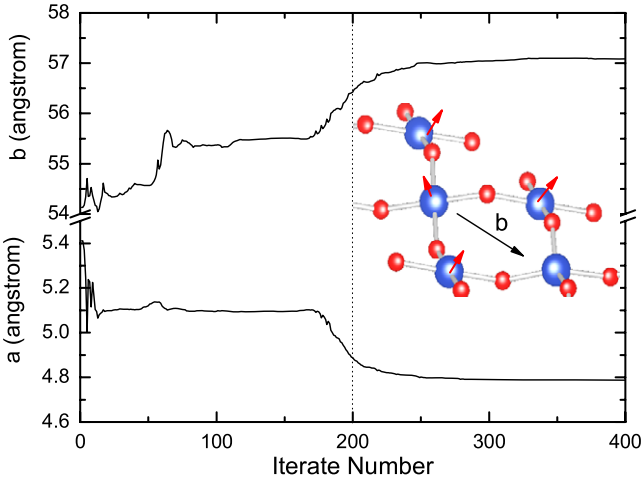


**Figure 5.** The changes in size of the cell along the $a$ axis and the $b$ axis with iteration number. The inset shows the tilting $CuO_2$ layer after about 300 iterations. The arrow $b$ illustrates the $b$ axis. The other small arrows show the tilting of the $CuO_2$ layer.

A $k$-point $2 \times 1 \times 1$ mesh and a mesh with only the Γ points are used in the corresponding calculations of electronic structures. The relaxed structure obtained by using Γ points shows most clearly the structural modulations in figure 4. We can see a modulated structure along the $b$ direction with the feature of 'missing-row' structures along the $a$ direction, which is very similar to the observations from scanning tunneling microscopy [15, 16]. We should note that there are no missing Bi atoms or O atoms. The 'missing-row' structure is induced by the short BiO bond length compared with those for the bonds in the neighboring perovskite-like structure. The modulation period is about $3b_0$–$4b_0$ which is smaller than the $\sim 5b_0$ in the model refined from x-ray studies and observed in STM experiments. The narrow size along the $a$ direction results in no reconstructions being found in figures 1 and 2. Thus our calculations with Γ points reproduce very well the STM observations, although with shorter modulation period. Additionally from figure 5, we found that the size of the slab along $a$ shrinks to a smaller value of about 4.79 Å and the size along $b$ increases from 55 to 57 Å; simultaneously the two $CuO_2$ planes tilt, with the angle 20°. The tilting and elongation of the $CuO_2$ layer, which are very common for cuprate high-temperature superconductors, can induce the formation of conducting strips in $CuO_2$ layers [25, 26]. Experimentally, when $CuO_2$ planes tilt the superconductor becomes a semiconductor [27], which is different from the findings of our calculations.

A larger slab including 600 atoms with size $2a_0 \times 10b_0$ on the $a$–$b$ plane is also used in our simulations. Very complex patterns of reconstructions of BiO surfaces are found in our simulations. The 'missing rows' or S-like structures are not found in the larger slab. The tilting of $CuO_2$ planes and large changes of lattice constants along the $a$ and $b$ directions in figure 5, which are necessary for forming 'missing rows', are not found in the simulations with the larger cell. The underlying reason may be that the corresponding relaxed or activated time for forming the 'missing row' is too long.

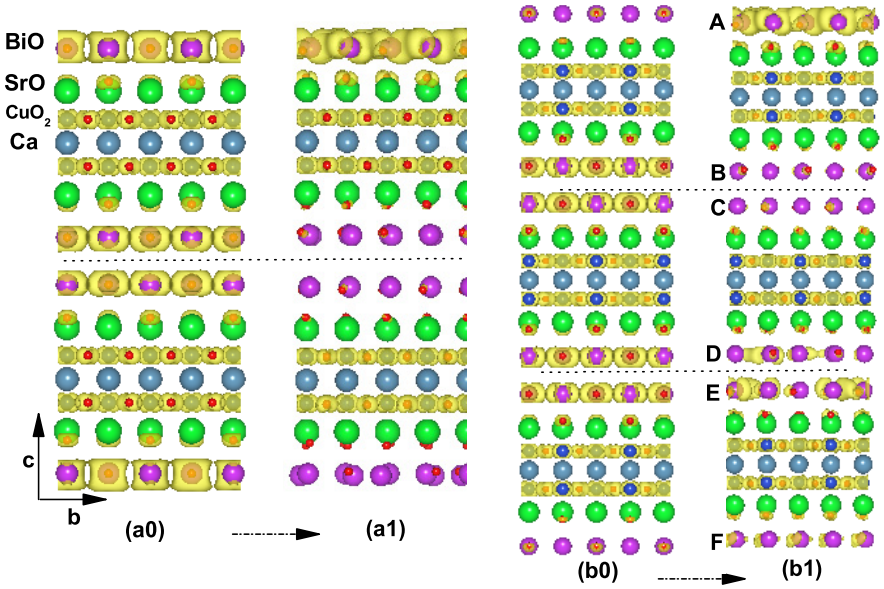


**Figure 6.** The non-relaxed structures of (a0) Model-240 and (b0) Model-360 (side view). The subfigures (a1) and (b1) show the corresponding relaxed structures of subfigures (a0) and (b0). The spatial LDOS around the Fermi energies, ±50 meV, are plotted in these figures with the iso-surface value 0.001 (1 $Å^{-3}$).

## 4. The reconstructions of BiO layers in the bulk of Bi2212

The x-ray experiments provided evidence of the reconstructions and modulations of BiO layers in the bulk of Bi2212 [12], just as in the surface BiO layers. The weak interactions between BiO layers make reconstructions of BiO layers easy compared with those in SrO and $CuO_2$ layers. In the following, we are going to investigate the reconstructions of internal BiO layers. We use two simulation cells with 240 atoms and 360 atoms, named Model-240 and Model-360 respectively. The sizes of Model-360 along the $a$ and $b$ directions are $2a_0$ and $2b_0$, shown in figure 6(b0). The slab includes three slab units along the $c$ direction, with a 15 Å empty space above the BiO surface if periodic boundary conditions are considered. Model-240 has a similar simulation cell; the difference is that there are two slab units along the $c$ axis shown in figure 6(a0). The small size along $a$ and $b$ means that we focus on the reconstructions of the BiO layer and ignore the modulations of BiO layers, which requires that at least one side of the simulation cell is longer than $5b_0$. In the process of structural optimization, the Γ point is used to sample the Brillouin zone in the corresponding electronic structure calculations. The more accurate electronic structures of the optimized structure are calculated using a $2 \times 2 \times 1$ $k$-point mesh.

The optimized structures are shown in figure 6(a1) for Model-240 and figure 6(b1) for Model-360. The six BiO layers in figure 6(b1) for Model-360 are plotted in figures 7(A)–(F). From these figures we can see that all BiO layers of the simulation cell are reconstructed after structural optimization. Two kinds of reconstructions, figures 7(D) and (F), have already appeared in figures 2(a) and (b) for the single-slab-unit model. A new reconstructed pattern exists in figures 7(A)–(C). The BiO-zigzag chains with orientation angle about 45° are related to the $a$ axis and parallel to the Cu–O bonds in the $CuO_2$ layer. The two nearest-neighbor BiO layers (C) and (B) have the same type of reconstruction. However one layer mirrors another layer. The reconstruction in figure 7(E) has patterns mixing figures 7(D) and (C). The nearest-neighbor (D) and (E) layers are different but the mixing type (E) layer has a $Bi_2O_2$ quadrilateral belonging to the type (D) layer. The reconstructions of Model-240 are very similar to the Model-360 ones.

Figure 6 presents the spatial LDOS of the non-relaxed structures ((a0), (b0)) and relaxed structures ((a1), (b1)) with energies around the Fermi energy, about ±50 meV. The spatially distributed LDOS of the BiO surface of non-relaxed Model-240 in figure 6(a0) is very small compared with that of non-relaxed Model-360 in figure 6(b0). However in the bulk, the LDOS of BiO layers are large for both non-relaxed models. For the relaxed and optimized structures of the two models, the spatially distributed LDOS of the BiO layers in the bulks are remarkably reduced to small values, as shown in figures 6(a1) and (b1). However the LDOS of the top BiO layers of both Model-240 and Model-360 increase upon structural relaxation. Like in figure 1 for the single-slab model, the pp$\sigma$ bonds between next-nearest-neighbor Bi atoms in the top surfaces are all parallel to Cu–O bonds for both models. From figure 8, the spatial LDOS of the top BiO layer (A) and that of the second BiO layer (B) beneath the surface of Model-360 are very different from each other. The top BiO layer (A) is electronically conducting and the second BiO layer (B) is insulating although they have similar reconstruction patterns.

It is well known that a BiO layer is metallic in the non-relaxed structure of Bi2212 in the calculations of density functional theory with LDA or GGA corrections to the exchange–correlation functional. The main contributions of BiO layers to the DOS at the Fermi energy come from the small

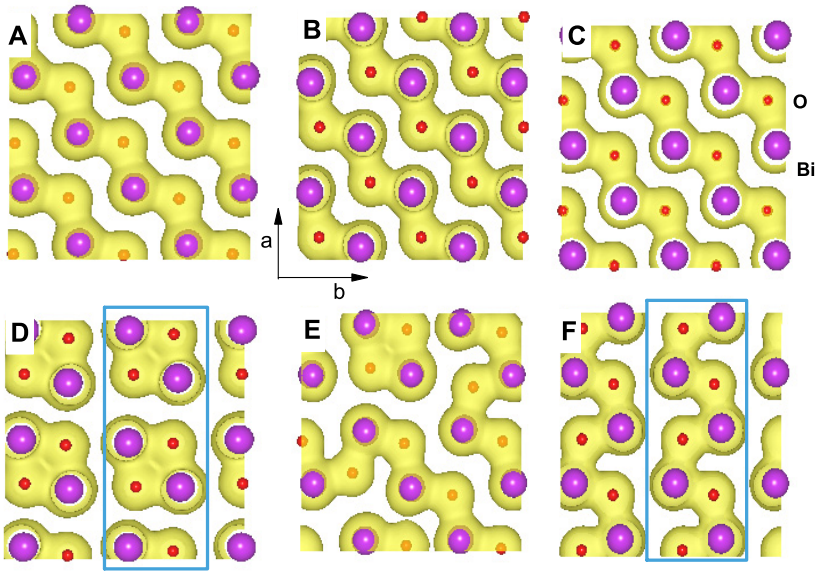


**Figure 7.** The electronic densities of six BiO layers in the relaxed structure of figure 6(b1) with 360 atoms (top view). As in figure 2, the iso-surfaces are plotted using the full densities of valence electrons with iso-value 0.02 (1 $Å^{-3}$).

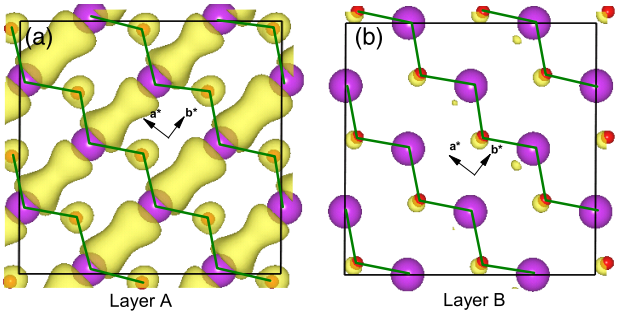


**Figure 8.** The spatial LDOS in A and B layers in figure 7 are plotted with energies around the Fermi energy, ±50 meV, with iso-surface value 0.001 (1 $Å^{-3}$). Two orthogonal arrows show the directions of Cu–O bonds beneath the BiO layer. The solid zigzag lines are guides to the zigzag Bi–O chains in the A and B layers in figures 7 and 6(b1).

pockets of Fermi surfaces near $\bar{M}$ point with the wavevector along the Cu–O bonds [18]. This means that there is lattice instability induced by the nesting properties of the Fermi surface near the $\bar{M}$ point, similar to the Peierls instability. The reconstructions of the A, B and C layers in figure 7 are created by this mechanism. We find that the B and C layers in the bulk become insulating or semiconducting as a result of a mechanism similar to the Peierls mechanism, but the reconstructions of the D, E and F layers are driven by a different nesting vector. For examples the nesting vectors driving the reconstructions of A, B, C layers and F layer in figure 7 are $q_A = q_B = q_C = \sqrt{2}(1, 1, 0)$ and $q_F = (0, 1, 0)$ (with unit $2\pi/a$) respectively. The top A layer with a similar reconstruction to the B and C layers is still metallic, although the charge distribution is very different from that of the non-relaxed structure. The residual metallic states in the top A and bottom F layers are correlated with the global distribution of the electronic density and sensitively dependent on the local environments of the BiO layers and thicknesses of the slabs. The metallic properties of the D and E layers become weak upon structural relaxations; however there are still residual metallic states. The reconstructions of BiO layers can lead to inhomogeneously distributed densities of carriers in the bulk and on the surface of Bi2212. The mirror effects of the periodic boundary condition along the $c$ axis are small because the results exhibit small changes when the thicknesses of the vacuum layers are increased. The inhomogeneous modulation of the charge distribution had been found in the x-ray observation; this was related to the nanometer charge distribution observed in STM experiments [17]. The contributions of BiO layers to the density of states at the Fermi surface will be further reduced if the modulations of BiO layers are produced at a larger length scale, just as presented in section 3.

## 5. Discussion and conclusion

The local densities of states (LDOS) of different atomic layers of Bi2212 are systemically calculated in this work. The LDOS $g(r)$ of the surface layer can be obtained by measuring the differential conductance $dI/dV \sim g(r)$ at position $r$ using the STM/STS technique. And the spatial LDOS map of the surface can be obtained by scanning the surface at fixed bias voltage [29]. Generally, the BiO surface is considered as semiconducting and makes no contribution to the density of states near the Fermi energy. This means that the top BiO surface makes no contribution to the LDOS map of the BiO surface at low bias voltage. Only at high bias voltage does the main contribution to the LDOS map come from the BiO surface. The STM/STS experiments found a modulating pattern in the LDOS map of the BiO surface at low bias voltage which has the same orientation as the $CuO_2$ layer beneath, with a 45° axis relative to the Bi–O bonds. The patterns in the LDOS

maps have been explained as traces of charge modulations of the $CuO_2$ layer beneath [30, 31]. Since the cleavage plane of Bi2212 is the BiO plane and the STM tip directly scans the BiO surface, the influence of the BiO surface on LDOS map cannot be ignored even at low bias voltage.

Our results show that some characteristics of the electronic and atomic structures of the $CuO_2$ layer beneath emerge in the BiO surface by structural reconstruction and modulation. The surface BiO layer can be metallic and the BiO layers in the bulk are insulating or semiconducting. The emerging Bi–Bi pp$\sigma$ conducting bonds in figures 1 and 8 are parallel to the Cu–O bonds beneath. The conducting strip on the BiO surface composed of Bi–Bi pp$\sigma$ bonds may contribute to the LDOS map of the BiO layer at low bias voltage. Thus the pattern of the LDOS map at low bias is probably not solely contributed by the $CuO_2$ layers beneath. In fact, the conducting strip in figure 1 will obscure the pattern because it is along the *a* axis with a 45° angle relative to the Cu–O bonds. From figure 8, the reconstruction of the top surface BiO layer (A) in Model-360 will form a charge modulation coinciding with the $CuO_2$ layer and enhance the LDOS map in STM/STS experiments at low bias voltage.

In summary, we have studied the formations of incommensurate modulations of the copper oxide high-temperature superconductor Bi2212 on the basis of *ab initio* density functional calculations. The formations of structural modulations are closely related to the reconstructions of the BiO surface by forming BiO-zigzag chains and $Bi_2O_2$ quadrilaterals along the *a* axis. The direction of modulation is along the *b* axis perpendicular to the BiO-zigzag chains. The modulation period is about $3b_0$–$4b_0$ which is shorter than the $4.7b_0$–$4.8b_0$ in the model refined and observed in experiments. The structural modulations are spontaneously formed not only in the BiO layer but also in the SrO and $CuO_2$ layers. Our simulations reconcile the observations using STM and x-ray diffraction, and provide a universal description for the formation of modulated structure of the BiO layer and surface.

## Acknowledgments

The authors thank Professor L J Zou for kindly reading and commenting on the manuscript. This work was run on the computers in the computing center of CASHIPS. The crystal structure figures were plotted using VESTA [28]. This work was financially supported by the Knowledge Innovation Program of the Chinese Academy of Sciences, the Special Funds for the Major State Basic Research Project of China (973) under Grant 2007CB925004 and the National Science Foundation of China under Grant 90503005.

## References

[1] Maeda H, Tanaka Y, Fukutomi M and Asano T 1988 *Japan. Appl. Phys.* **27** L209
[2] Gao Y, Lee P, Coppens P, Subramania M A and Sleight A W 1988 *Science* **241** 954
[3] Pan S H *et al* 2001 *Nature* **413** 282
[4] Bordet P, Capponi J J, Chaillout C, Chenavas J, Hewat A W, Hewat E A, Hodeau J L, Marezio M, Tholence J L and Tranqui D 1988 *Physica* C **153–155** 623
Bordet P, Capponi J J, Chaillout C, Chenavas J, Hewat A W, Hewat E A, Hodeau J L, Marezio M, Tholence J L and Tranqui D 1988 *Physica* C **156** 189
[5] Li X M, Li F H, Luo H Q, Fang L and Wen H H 2009 *Supercond. Sci. Technol.* **22** 065003
[6] Mo Y D, Cheng T Z, Fan H F, Li J Q, Sha B D, Zheng C D, Li F H and Zhao Z X 1992 *Supercond. Sci. Technol.* **5** 69
[7] Le Page Y, McKinnon W R, Tarascon J-M and Barboux P 1989 *Phys. Rev.* B **40** 6810
[8] Petricek V, Gao Y, Lee P and Coppens P 1990 *Phys. Rev.* B **42** 387
[9] Yamamoto A, Onoda M, Takayama-Muromachi E and Izumi F 1990 *Phys. Rev.* B **42** 4228
[10] Levin A A, Smolin Yu I and Shepelev Yu F 1994 *J. Phys: Condens. Matter* **6** 3539
[11] Jakubowicz N, Grebille D, Hervieu M and Leligny H 2001 *Phys. Rev.* B **63** 214511
[12] Gladyshevskii R E and Flükiger R 1996 *Acta Crystallogr.* B **52** 38
[13] Calestani G, Rizzoli C, Francesconi M G and Andreetti G D 1989 *Physica* C **161** 598
[14] Sedykh V, Shekhtman Sh V, Smirnova I S, Bagautdinov B Sh, Suvorov E V and Dubovitskii A V 2003 *Physica* C **390** 311
[15] Slezak J A, Lee J, Wang M, McElroy K, Fujita K, Andersen B M, Hirschfeld P J, Eisaki H, Uchida S and Davis J C 2008 *Proc. Natl Acad. Sci. USA* **105** 3203
[16] Shan L, Ejov A, Volodin A, Moshchalkov V V, Wen H H and Lin C T 2003 *Europhys. Lett.* **61** 681
[17] Castellan J P, Gaulin B D, Dabkowska H A, Nabialek A, Gu G, Liu X and Islam Z 2006 *Phys. Rev.* B **73** 174505
[18] Bellini V, Manghi F, Thonhauser T and Ambrosch-Draxl C 2004 *Phys. Rev.* B **69** 184508
[19] He Y, Nunner T S, Hirschfeld P J and Cheng H-P 2006 *Phys. Rev. Lett.* **96** 197002
[20] Singh D J and Pickett W E 1995 *Phys. Rev.* B **51** 3128
[21] He Y, Graser S, Hirschfeld P J and Cheng H-P 2008 *Phys. Rev.* B **77** 220507(R)
[22] Kresse G and Joubert D 1999 *Phys. Rev.* B **59** 1758
[23] Blöchl P E 1994 *Phys. Rev.* B **50** 17953
[24] Perdew J P, Burke K and Ernzerhof M 1996 *Phys. Rev. Lett.* **77** 3865
[25] Bianconi A, Saini N L, Lanzara A, Missori M, Rossetti T, Oyanagi H, Yamaguchi H, Oka K and Ito T 1996 *Phys. Rev. Lett.* **76** 3412
Bianconi A 1994 *Physica* C **235–240** 269
[26] Cui S F, Li C R, Mai Z H, Xiong J W, Zhao Z X, Wang Y T and Hatton P D 1999 *Supercond. Sci. Technol.* **12** 587
[27] Samukawa G, Kambe S, Yoshida C, Ohshima S and Ishii O 1997 *Physica* C **282–287** 937
[28] Momma K and Izumi F 2008 *J. Appl. Crystallogr.* **41** 653
[29] Hoffman J E, McElroy K, Lee D-H, Lang K M, Eisaki H, Uchida S and Davis J C 2002 *Science* **297** 1148
[30] Vershinin M, Misra S, Ono S, Abe Y, Ando Y and Yazdani A 2004 *Science* **303** 1995
[31] Fang A, Howald C, Kaneko N, Greven M and Kapitulnik A 2004 *Phys. Rev.* B **70** 214514